 ©2013 Kvantovaya Elektronika and Turpion Ltd

INTERACTION OF LASER RADIATION WITH MATTER

PACS numbers: 68.03.Fg; 07.07.Df; 41.20.Cv; 42.55.–f
DOI: 10.1070/QE2013v043n01ABEH014923

Spatial separation and motion of electric charges arising due to the interaction of high-power IR laser radiation with water

N.N. Il'ichev, L.A. Kulevskii, P.P. Pashinin

Abstract. **We have studied temporal and amplitude characteristics of the electrical signal arising under irradiation of the free water surface by a 2.94-μm high-power laser. The investigations have been conducted using a specially designed electrode system, which makes it possible to record the motion of the electric charge after the end of the laser pulse. We have measured the dependences of the signal parameters on the radiation energy density at the water surface.**

Keywords: *interaction of laser radiation with water, electric charge, diffusion separation.*

1. Introduction

We found [1] that when the water surface is exposed to 2.92-μm high-power laser radiation, a time-dependent electrical signal arises on the electrodes located near the interaction region. Having investigated this phenomenon both theoretically and experimentally the authors of [2–5] came to the conclusion about the importance of the contribution of the motion of charges in the evaporated water to the formation of an electrical signal. The pulse shape, as noted already in [1], depends on the conditions of registration, such as the values of the input resistance and capacitance of the oscilloscope, shape and arrangement of the electrodes with respect to the interaction region of radiation with the water surface, as well as on external static fields. The aim of this work is to study temporal and amplitude characteristics of the electrical signal arising under irradiation of the free water surface by 2.94-μm high-power laser pulses in the case of a special shape of the electrodes. The selected registration scheme has made it possible to record the charge motion after such an exposure, as well as to measure its sign and magnitude.

2. Electrical signal recording scheme

Figure 1 shows an electrode system (hereafter, a cell), used to record the electrical signal. This system consisted of two metal coaxial (signal) cylinders separated by a gap 0.1 to 0.4 mm. One of the cylinders was filled with water, onto which surface IR radiation was incident. The water level relative to the edge of the cylinder could be varied. Both signal cylinders were placed in a grounded coaxial cylinder of a larger diameter.

In previous papers [1–4] the electrical signal was recorded by using two coaxial rings, whose height was significantly less than their diameter, which led to an uncontrolled influence of metal parts of the setup, as well as of alternating and static electric fields on the magnitude and shape of the signal. A specific feature of the new electrode system consisted in the fact that the electrical signal appeared only when a moving charge crossed the gap between the internal cylinders. By varying the distance between the laser-irradiated surface of the water inside the bottom cylinder and the gap between the cylinders, it is possible to measure the spatial distribution of the charge, its velocity, and the sign. The geometry of the electrodes allows one to calculate with good accuracy the potentials at the electrodes as a function of the charge distribution inside the cylinders.

3. Calculation of the potential distribution in the cell

Consider the problem for the scheme shown in Fig. 2. In the region $-\infty < z \leqslant z_0$ a conducting infinitely long cylinder with an inner radius a is filled with a medium with permittivity ε_2, and in the region $z_0 < z < \infty$ – with a medium with permittivity ε_1. Let an infinitely thin (in the z-direction) and radially uniform flat layer with a total charge q be located at point $z = z_1$ and other free of charges be absent. We believe that the charge distribution is fixed. We find the potential inside the cylinder, which is produced by this charge. The equation for this problem in cylindrical coordinates and boundary conditions have the form:

$$\frac{1}{r}\frac{\partial}{\partial r}r\frac{\partial U}{\partial r}+\frac{\partial^2 U}{\partial z^2}=-\frac{\sigma(r)}{\varepsilon_0\varepsilon(z)}\delta(z-z_1),$$

$$\sigma(r)=\begin{cases}\dfrac{q}{S_a}, & r<a,\\ 0, & r=a,\end{cases} \qquad (1)$$

$$\varepsilon(z)=\begin{cases}\varepsilon_1, & z>z_0,\\ \varepsilon_2, & z\leqslant z_0,\end{cases}$$

$$U(r=a,z)=0.$$

Here $U(r, z)$ is the potential inside the cylinder; $\sigma(r)$ is the surface density of the charge in the plane $z = z_1$; a is the radius of the cylinder; ε is permittivity; ε_0 is the permittivity of vacuum; $\delta(z)$ is the delta function; and $S_a = \pi a^2$ is the cross-sectional

N.N. Il'ichev, L.A. Kulevskii, P.P. Pashinin A.M. Prokhorov General Physics Institute, Russian Academy of Sciences, ul. Vavilova 38, 119991 Moscow, Russia;
e-mail: ilichev@kapella.gpi.ru, pashinin@gpi.ru

Received 8 June 2012; revision received 29 July 2012
Kvantovaya Elektronika **43** (1) 47–54 (2013)
Translated by I.A. Ulitkin

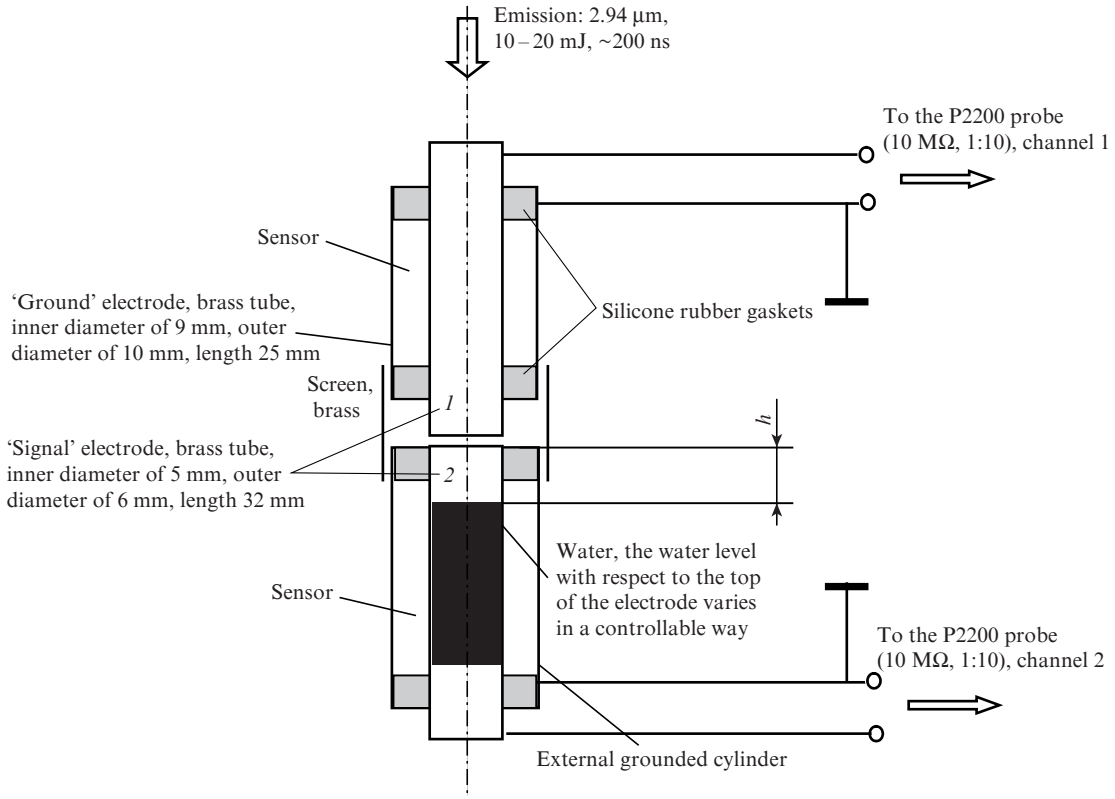

Figure 1. Scheme of the cell for measuring the electrical signal produced in the interaction of laser radiation with the water surface.

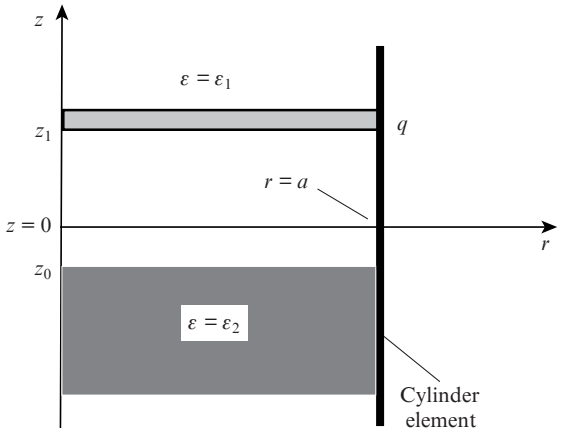

Figure 2. Infinite conducting cylinder of radius a. The charge q is distributed in the form of an infinitely thin, radially uniform layer at $z = z_1$; the surface of the dielectric interface is at $z = z_0$.

area of the cylinder. Due to the azimuthal symmetry of the problem we assume that the solution is independent of the azimuthal angle. Let us represent the potential above the surface of the interface between the dielectrics as the sum of the two potentials, the second potential resulting from reflection of the charge by the interface surface. We seek the solution in the form

$$U(r,z) = \begin{cases} U_0(r, z - z_1) + B_x U_0(r, z + z_1 - 2z_0), & z \geqslant z_0, \\ C_x U_0(r, z - z_1), & z \leqslant z_0, \end{cases}$$

$$U_0(r,z) = \sum_n A_n \exp\left(-\gamma_n \frac{|z|}{a}\right) J_0\left(\gamma_n \frac{r}{a}\right), \tag{2}$$

where $J_0(x)$ is the zero-order Bessel function, and γ_n is the nth root of the equation $J_0(x) = 0$. The coefficients are found from the charge distribution given in (1) in the plane $z = z_1$:

$$A_n = \frac{aq}{S_a \varepsilon_0 \varepsilon_1 \gamma_n^2 J_1(\gamma_n)}. \tag{3}$$

In this case, the density of the charge distribution has a discontinuity at point $r = a$. The case, when the charge distribution is continuous along the radius, is discussed in the Appendix. From the condition of continuity of the potential we obtain at $z = z_0$

$$1 + B_x = C_x, \tag{4}$$

From the condition of continuity of the normal component of the induction, we find at $z = z_0$

$$1 - B_x = \frac{\varepsilon_2}{\varepsilon_1} C_x. \tag{5}$$

Solving the system of equations (4) and (5), we find the coefficients

$$B_x = \frac{\varepsilon_1 - \varepsilon_2}{\varepsilon_1 + \varepsilon_2},$$

$$C_x = \frac{2\varepsilon_1}{\varepsilon_1 + \varepsilon_2}. \tag{6}$$

And, finally, the desired solution takes the form

$$U(r,z)=\begin{cases}\sum\limits_{n=1}^{\infty}A_nJ_0\left(\gamma_n\frac{r}{a}\right)\left[\exp\left(-\gamma_n\frac{|z-z_1|}{a}\right)\right.\\ \left.+\frac{\varepsilon_1-\varepsilon_2}{\varepsilon_1+\varepsilon_2}\exp\left(-\gamma_n\frac{z+z_1-2z_0}{a}\right)\right], & z\geqslant z_0,\\ \frac{2\varepsilon_1}{\varepsilon_1+\varepsilon_2}\sum\limits_{n=1}^{\infty}A_nJ_0\left(\gamma_n\frac{r}{a}\right)\exp\left(-\gamma_n\frac{|z-z_1|}{a}\right), & z\leqslant z_0.\end{cases} \quad (7)$$

From (7) we can find the surface density of the induced charge on the inside of the cylinder at $r = a$:

$$\sigma_s(z,z_0,z_1,q)=\begin{cases}-\frac{q}{S_a}\sum\limits_{n=1}^{\infty}\frac{1}{\gamma_n}\left[\exp\left(-\gamma_n\frac{|z-z_1|}{a}\right)+\frac{\varepsilon_1-\varepsilon_2}{\varepsilon_1+\varepsilon_2}\right.\\ \left.\times\exp\left(-\gamma_n\frac{z+z_1-2z_0}{a}\right)\right], & z\geqslant z_0,\\ -\frac{q}{S_a}\frac{2\varepsilon_1}{\varepsilon_1+\varepsilon_2}\sum\limits_{n=1}^{\infty}\frac{1}{\gamma_n}\exp\left(-\gamma_n\frac{|z-z_1|}{a}\right), & z\leqslant z_0.\end{cases} \quad (8)$$

The solution to expression (8) is also valid if the charge lies on the surface of the interface between the dielectrics.

Consider now the problem when a thin distributed charge $-q$ is located at point $z = z_1$, and an infinitely thin distributed charge $+q$ is located on the water surface ($z = z_0$) (Fig. 3). In this case, the potential is the sum of the potentials of each of the charges, and the charge distribution on the cylinder surface is found by means of expression (8):

$$\sigma_\Sigma(z,z_0,z_1,q) = \sigma_s(z,z_0,z_1,-q) + \sigma_s(z,z_0,z_0,q). \quad (9)$$

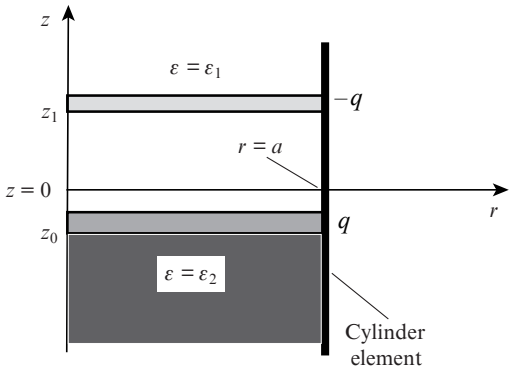

Figure 3. Infinite conducting cylinder of radius a. The charge q in the cylinder is distributed in the form of an infinitely thin, radially uniform layer on the surface of the dielectric at $z = z_0$, where $z_0 < 0$, and the charge $-q$ is distributed in the form of a thin layer above the water surface at $z = z_1$.

For the cases when the charge $+q$ is on the water surface and the charge $-q$ is at point $z = z_1$, we find from (9) the values of the charges Q_1 and Q_2, induced at the upper ($z > 0$) and lower ($z < 0$) parts of the inner surface of the cylinder:

$$Q_1 = \int_0^{\infty}\sigma_\Sigma(z,z_0,z_1,q)2\pi a\,dz,\ z>0,$$
$$Q_2 = \int_{-\infty}^{0}\sigma_\Sigma(z,z_0,z_1,q)2\pi a\,dz,\ z<0. \quad (10)$$

We assume that the cylinder is cut into two half-cylinders $z \leqslant 0$ and $z \geqslant 0$, which are now isolated from each other. Let us also assume that the charges on these half-cylinders are given by formula (10). We take into account that the charges on the inner and outer sides of each half-cylinder are equal in magnitude and opposite in sign. Then, we can find the potentials of these half-cylinders relative to the 'ground' point:

$$U_1 = -\frac{Q_1}{C_1},\ U_2 = -\frac{Q_2}{C_2},\ U_{12} = U_1 - U_2, \quad (11)$$

where C_1 and C_2 are the capacitances between the central half-cylinder and the grounded outer electrode (Fig. 1). The charge distribution on the outside of the half-cylinders is determined by a specific arrangement of the grounded conductors surrounding the cylinder. Solution (11) for the potentials is approximate. It does not take into account the fact that at $z = 0$ there must be a potential jump to which some charge corresponds at the interface of the section. But if the mutual capacitance of the two cylinders is much less than the capacity C_1 or C_2, this charge can be neglected.

In our case, the length L of each half-cylinder was ~30 mm, and not infinite, as is customary in the calculation; however, because the inner radius of the cylinder is a = 2.5 mm and $L \gg a$, this approximation is good enough, which is confirmed by the calculation in accordance with (8) – (11). Expression (7) also shows that if the charge moves along the z axis, the potential starts to change when the charge is near $z = 0$, at a distance $\Delta z \sim a/\gamma_1$ ($\gamma_1 = 2.405$). In this case, the distance is about 1 mm. Let us estimate the impact of the mutual capacitance of the cylinders on the error of the charge measurement.

4. Equivalent circuit of the cell

For the equivalent electrical circuit of a real cell (Fig. 4) we can write the system of equations:

$$q = q_1 + q_2,\ q_1 = C_{12}U_{12},\ q_2 = C_{10}U_{10} = -C_{20}U_{20},$$
$$U_{12} = q_2\left(\frac{1}{C_{20}}+\frac{1}{C_{10}}\right),\ q_2 = q\left[1 + C_{12}\left(\frac{1}{C_{20}}+\frac{1}{C_{10}}\right)\right]^{-1}. \quad (12)$$

By solving this system for the voltage between the electrodes (*1*) and (*2*) we obtain

$$U_{12} = q(1/C_{20} + 1/C_{10})\left[1 + C_{12}\left(\frac{1}{C_{20}}+\frac{1}{C_{10}}\right)\right]^{-1}. \quad (13)$$

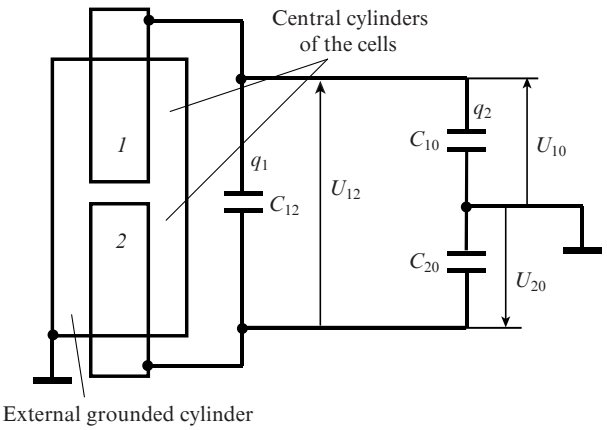

Figure 4. Equivalent electric circuit of the cell.

Thus, knowing the voltage U_{12}, and the capacities C_{10}, C_{20}, and C_{12}, we can find the charge q.

In our case, the capacitance between the central electrode and the outer cylinder is $C_x = 7 \pm 0.5$ pF (measured by an R577 ac bridge). The input capacitance of the P2200 probe is $C_{in} = 16$ pF, and $C_{10} = C_{20} = C_x + C_{in}$. The measured capacitance between the inner cylinders (*1*) and (*2*) was found to be 1.5 pF. Thus, $C_{20} = C_{10} = 23$ pF, and $C_{12} = 1.5$ pF. And as in our case $C_{12} \ll C_{10}, C_{20}$, the capacitance C_{12} is neglected below in the calculations.

5. Influence of the load resistance on the signal shape

Since $C_{12} \ll C_{10}, C_{20}$, the signals from the electrodes (*1*) and (*2*) (Fig. 4) can be considered separately, and the equivalent electrical circuit with the load R for a single electrode taken into account can be schematically shown in the following way (Fig. 5). The moving charges in our case are the source of the current. For this circuit, we can write the equations:

$$I = I_1 + I_2,\ U_C = \frac{1}{C}\int I_1 \mathrm{d}t,\ U_R = RI_2,\ U_R = U_C = U. \quad (14)$$

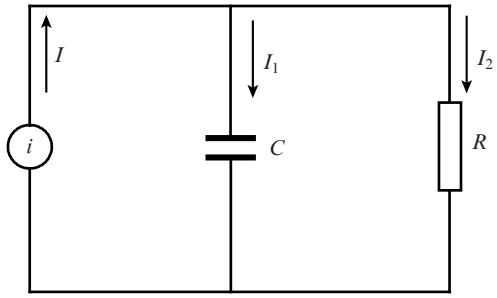

Figure 5. Circuit for measuring the electrical signal.

From (14) we obtain an equation relating the current and voltage with the load resistance:

$$I = C\frac{\mathrm{d}U}{\mathrm{d}t} + \frac{1}{R}U. \quad (15)$$

From equation (15) we can find the charge

$$q(t) = \int_0^t I(t')\mathrm{d}t' = C\left(U + \frac{1}{RC}\int_0^t U(t')\mathrm{d}t'\right). \quad (16)$$

Here R is the input resistance of the probe (in our case, 10 MΩ); $U(t)$ is the voltage measured in the experiment; and $C = C_{20} = C_{10}$. The time constant $\tau = RC$ was determined by the discharge time of the capacitance C through the input resistance R and was found to be 230 μs. The voltage U_1, which would have been recorded at an input resistance $R \to \infty$, is given by the expression

$$U_1(t) = U(t) + \frac{1}{\tau}\int_0^t U(t')\mathrm{d}t'. \quad (17)$$

Thus, knowing the time dependence of the voltage at a known input resistance R, we can determine the time dependence of the signal for a large input resistance, if we know the time constant τ. This approach allows one to avoid the use of an electronic repeater with a high input resistance. The accuracy of reconstruction depends on the time interval over which the measurements are conducted; the distance is defined as $(3 - 5)\tau$. Expression (17) was used for signal processing.

6. Experimental results

Figure 6 shows typical oscillograms of electrical signals measured using the cell shown in Fig. 1 and DPO 7254 oscillo-

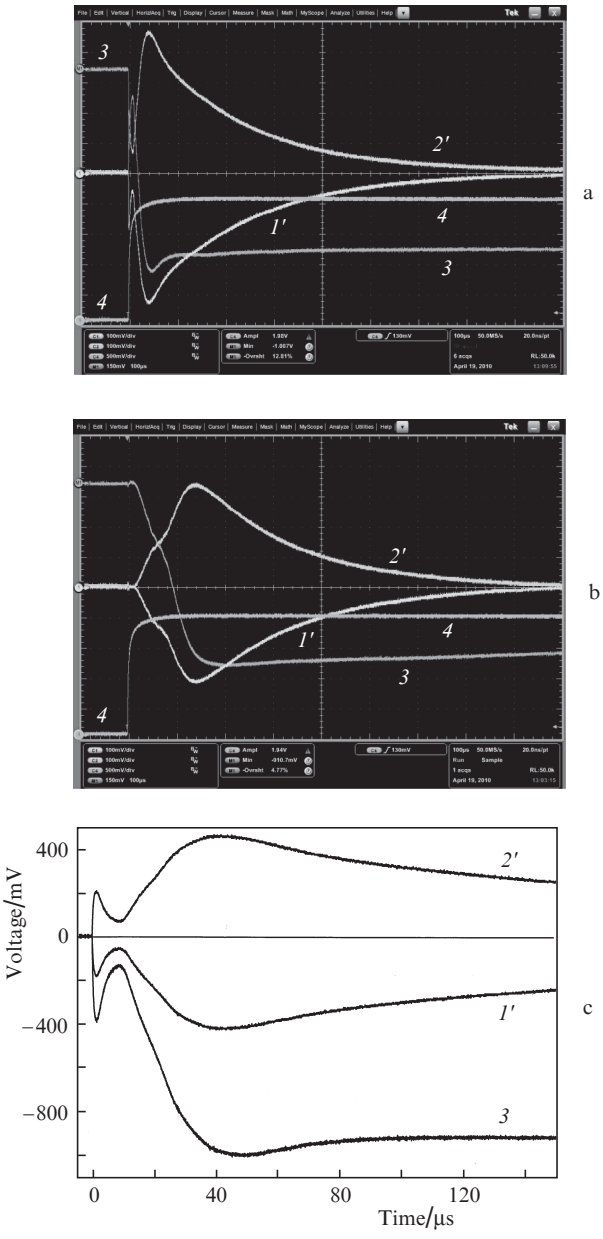

Figure 6. Typical oscillograms of the electrical signals recorded by the cell shown in Fig. 1, when the water level is (a) close to the upper edge of the lower cylinder and (b) 5 mm below the edge; curves (*1′*) and (*2′*) show the signals from the electrodes (*1*) and (*2*) (their tracks before the arrival of the electric pulse coincide), curve (*3*) demonstrates the mathematical processing of the difference between the signals (*1′*) and (*2′*) by formula (17), curve (*4*) is the signal from the photodetector which is proportional to the pulse energy; panel (c) is the initial part of the oscillogram (Fig 6a) 'stretched' along the horizontal axis.

scope. Oscillogram (*1′*) is a signal from the upper electrode (*1*) (Fig. 1), which has a negative polarity; oscillogram (*2′*) shows a signal from the lower water-filled electrode (*2*), which has a positive polarity. Oscillogram (*3*) is a difference between signals (*1′*) and (*2′*), processed according to formula (17) at $\tau = 230$ μs; oscillogram (*4*) is a signal from the photodetector, the maximum value of which is proportional to the laser energy. Oscillogram (*3*) in Fig. 6a corresponds to the case when the water level coincides with the upper edge of the lower cylinder ($z_0 = 0$). One can see the first peak of duration 2–3 μs and a dip (at $t \approx 5$ μs), followed by the signal reaching a constant level (plateau). The shape of the signal depends on the position of the level of water with respect to the upper edge of the bottom electrode. Signals in Fig. 6b, obtained at a water level offset by 5 mm from the top edge of the cylinder, demonstrate this fact. One can see that the amplitude of the first peak decreases, the time needed for the signal to reach the plateau increases, and the voltage on the plateau depends weakly on the water level. It should be noted that with decreasing water level only the amplitude of the first peak changes, and its temporal characteristics remain the same.

We have measured the dependences of the amplitude of the first peak and the plateau voltage on the position of the water level (Fig. 7). Below by the amplitude of the first peak and the plateau voltage is meant the difference between the signals (*1′*) and (*2′*), processed with the help of (17) at $\tau = 230$ μs. The points in Fig. 7a show the experimental dependence of these signals on the position of the water level with respect to the top of the cylinder (*1*). With lowering the water level, the amplitude of the first peak tends to zero. The points in Fig. 7b show the experimental dependence of the plateau voltage on the water level. One can see that the magnitude of the signal is almost independent of the water level.

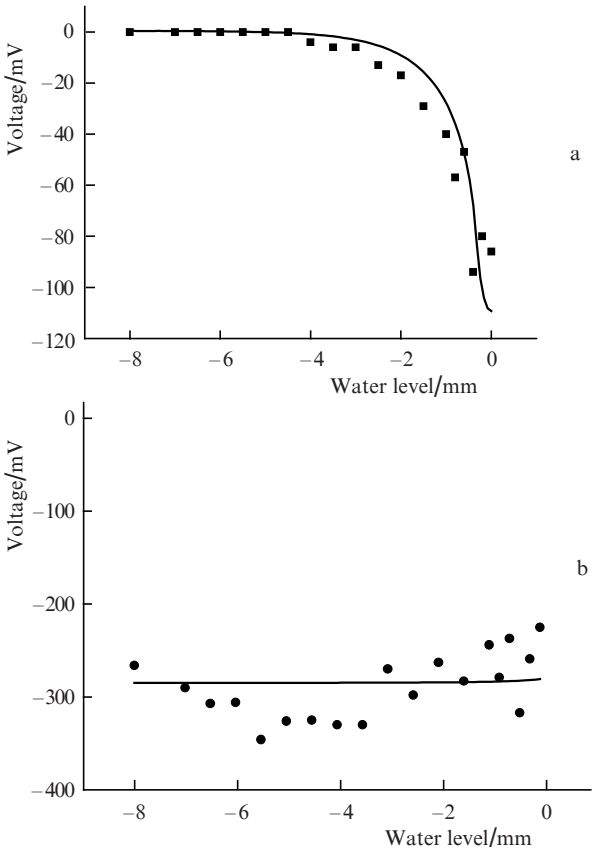

Figure 7. Dependences of (a) the amplitude of the first peak and (b) plateau voltage on the level of the water with respect to the edge of the lower cylinder; points are the experiment, solid lines are the calculation.

The dependences of the amplitude of the first peak and the plateau of electrical signals on the laser pulse energy are shown in Fig. 8. One can see that as the energy increases the signal amplitudes grow almost linearly. The signal appearance thresholds were 6.0 mJ and 5.4 mJ for the first peak and the plateau, respectively. These values corresponded to the energy densities of 0.22 and 0.19 J cm^{-2}. Because these values are close, one would assume that the difference between them is within the accuracy of the measurements; however, when the laser pulse energy decreases near the signal appearance threshold, the oscillograms clearly show that the signal is at maximum without a dip, i.e., the first peak disappears.

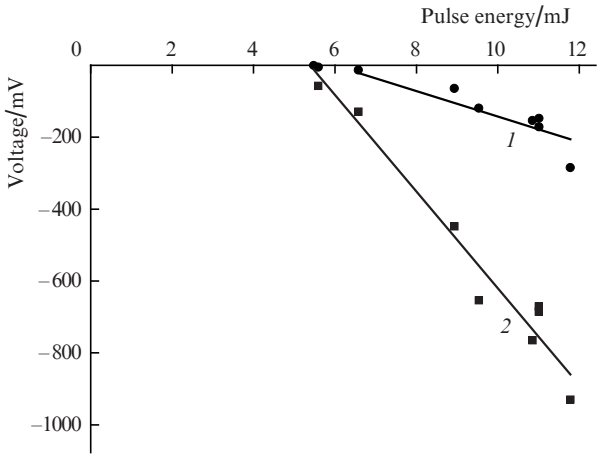

Figure 8. Dependence of the amplitude of the first peak (*1*) and the plateau voltage (*2*) on the laser pulse energy. Points are the experimental data, solid lines are the result of the linear least-squares approximation. The signal appearance thresholds of 6.0 and 5.4 mJ correspond to the energy density of ~0.2 J cm^{-2}; the area of the radiation spot on the surface is 0.028 cm^2.

It is also necessary to pay attention to the different slopes of the straight lines of the linear approximation of the amplitude of the first peak and the plateau voltage.

7. Discussion of the results of the experiment

Measurement of the electrical signal at the initial stage of development (we do not present here the corresponding oscillograms in order not to overload the text) shows that it emerges during the laser pulse action. The time of the electrical signal appearance depends on the energy density of radiation at the water surface, and when the energy density increases, it is shifted to the beginning of the pulse. By the end of the pulse the value of the signal is a fraction of its maximum value, which is reached much later (after 20–40 μs), and within the laser pulse only a monotonic increase in the signal takes place. This suggests that the charge separation occurs during the laser pulse and the subsequent behaviour of the electrical signal is associated with the motion of separated charges in the gas phase. This and the analysis of the oscillograms shown in Fig. 6 indicate that during the laser pulse

action a positive charge remains on the surface of the water, and a negative charge equal to the positive one in modulus is carried out to a gaseous medium (water vapour) above the water surface. This medium has a high temperature and pressure exceeding the pressure of the surrounding atmosphere, which leads to the formation of a shock wave in the atmosphere, and after the collapse of the shock wave – to the flow of water vapour away from the water surface, which carries away a negative charge located in the vapour. The time dependence of the measured signal reflects the characteristics of motion of charged water vapour.

We can single out two stages: the formation of the first peak and the formation of a plateau when the signal reaches a constant level. Let us analyse the signal, which is formed due to the charge motion from the water surface. The time for the signal output to a constant level depends on the initial water level (see Fig. 6). We can assume that the amplitude of the signal at the plateau is independent of the water level (see Fig. 7b), i.e., the signal is generated by a charge (under constant exposure conditions) whose value does not depend on the water level. When a charge moves from the surface to the top of the lower electrode, the charge is never lost. When a charge moves inside the upper electrode, the signal should not change. The solid line in Fig. 7b is the result of the calculation with the help of expression (11), which allows one to find the magnitude of the charge. It is assumed in the calculation that the positive charge is on the surface of water, and the negative charge is inside the upper cylinder, at a large distance from the interface between the two cylinders. The sum of these charges is zero. The calculation helps to find the dependence of the difference of the potentials between the upper and lower electrodes on the water level. The problem is regarded as static, since the characteristic times of the processes (~0.5 μs) are much longer than the time (~0.5 ns) for the light to pass a distance comparable to the size of the electrode system. The solid line presented in Fig. 7b is obtained when the value of the charge carried away from the water surface is equal to -3.2×10^{-12} C (2×10^7 charges of an electron). We assumed in the calculations that the permittivity of vapour is $\varepsilon_1 = 1$ and the permittivity of water is $\varepsilon_2 = 70$ (see, for example, [6]).

The time needed for the signal to reach the plateau depends on the water level, which allows one to estimate the characteristic velocity of motion of charged vapour at this stage (it can be estimated from Fig. 6b). In this case, the water was 5 mm below the edge of the electrode, and the time needed for the signal to reach the plateau was ~150 μs, and hence the average velocity v of the charge was ~33 m s^{-1}, i.e., at this stage of the process the gas velocity was significantly lower that the velocity of sound.

The amplitude of the first peak depends on the position of the water level from the top edge of the lower electrode (Fig. 7a). These data can be interpreted as follows. The charge rises to a certain distance above the water surface, and then moves in the opposite direction, thereby forming a maximum signal. This can be explained by the dependence of the signal amplitude on the water level: with increasing distance from the surface to the edge of the electrode the signal amplitude decreases. Calculations were performed using (11). It was assumed in the calculations that there are two charges: one (positive) is on the surface of water, and the second (negative) is at some distance above it. The sum of the charges is equal to zero. Thus, we seek the dependence of the difference of the potentials between the upper and lower cylinders on the water level at a fixed distance between the charges. The charge was taken from the previous calculations of the signal on the plateau (-3.2×10^{-12} C is the charge above the water surface). The solid curve in Fig. 7a shows the result of the calculation when distance between the charges is 0.325 mm. One can see that it satisfactorily describes the experimental data.

Knowing the distance (0.325 mm), which the charge passes during the formation of the first peak, and the time needed to reach the maximum (1 μs), we can estimate the velocity of the charge motion: $v \sim 330$ m s^{-1}, which corresponds to the speed of sound in air at room temperature. The energy density of the laser radiation on the surface of the water in this case is ~0.4 J cm^{-2}. It should be noted that the time needed to reach the maximum of the first peak depends on the radiation energy density at the water surface.

The physical mechanism of the formation of the first peak is unclear at present. The signal maximum is reached 1 – 2 μs after the laser pulse action. As a possible mechanism of its appearance, we could suggest the following. The transverse dimensions of the spot on the water are limited and because the gas of the surrounding atmosphere is at rest, it slows down the vapour jet. This can result in the formation of vapour motion, similar to the 'toroidal vortex' (see, for example, [7]). At the stage of the formation of a charged 'vortex', there appears the first peak. Then the 'vortex' moves in the ambient atmosphere, gradually stopping.

Consider now the dependence of the signal amplitude on the pulse energy. One can see from Fig. 8 that the signal appears when the energy (or energy density) exceeds the threshold value. This fact was first observed in [2], where the threshold was found to be 0.23 J cm^{-2}. The charge separation due to exposure of the water surface to the laser radiation is naturally associated with the process of intensive evaporation. A rough estimate of the energy density, when intensive evaporation begins by heating water to 100°C at a pressure of the surrounding gas equal to 1 atm, yields a value of ~0.04 J cm^{-2} (the heat capacity, 4.2 J g^{-1} deg^{-1}; the density, 1 g cm^{-3}; the coefficient of water absorption at a wavelength of 2.94 μm, 10^4 cm^{-1}), which is almost five times less than that observed in the experiment. This discrepancy indicates that this simple estimate is too rough and the threshold of the intensive evaporation should be assessed more accurately. In papers [4, 5] the electrical signal appearance threshold was associated with the explosive (bulk) boiling of water. It is also possible that, under the action of high-power radiation, the water is bleached [8–10], which leads to a decrease in the absorption coefficient, and consequently, to an increase in the amount of heated water and an increase in the energy density required for heating. The energy density, at which absorption saturates, is estimated at 0.1 J cm^{-2} [8].

Now we estimate the possibility of the diffusion mechanism of charge separation in water. Radiation is absorbed in the medium at a distance equal to the inverse absorption coefficient. If we assume that at each point the ion product of water is equal to the equilibrium value, then there is a concentration gradient H^+ and OH^- near the surface of the water. The diffusion coefficients of these ions are different, which should lead to different values of the flow of ions into the water. And, therefore, a flow of charged vapour should be carried away from the water surface. Since the diffusion coefficient of H^+ (D_H) exceeds the diffusion coefficient of OH^- (D_{OH}) [11, 12], the vapour flow from the water surface is negatively charged, in qualitative agreement with experimental data. The above argument does not account for the existence

of thermal diffusion, whose role due to a significant temperature gradient must be considered.

In addition, according to calculations [13, 14], the temperature maximum during intensive evaporation is reached at some distance (~0.1 μm) from the water surface (in its column), and under certain conditions, the explosive boiling is possible in the region of the temperature maximum. In our analysis we do not take this fact into account.

Since the temperature dependences of the diffusion coefficients and the ionic product of water are known [11], the measured excess of charged particles passed through the surface during the pulse action makes it possible to estimate the temperature of the water surface exposed to laser radiation.

The difference between the number of negatively and positively charged particles passing through the surface of the water during the pulse action can be estimated from the expression

$$N = -(D_{\mathrm{H}} - D_{\mathrm{OH}})\frac{\mathrm{d}n^{\pm}}{\mathrm{d}x} s\tau_{\mathrm{p}} = (D_{\mathrm{H}} - D_{\mathrm{OH}})s\tau_{\mathrm{p}}\alpha_0 n^{\pm},$$

where α_0 is the absorption coefficient of water; $n^{\pm}$ is the concentration of positive and negative ions on the water surface, which is determined by the product ion; τ_{p} is the pulse duration; and s is the area of the laser spot on the water surface. Let us substitute into this expression the values corresponding to the experimental conditions: $s = 0.028$ cm^2, $\tau_{\mathrm{p}} = 200$ ns, $D_{\mathrm{H}} = 9.319\times10^{-5}$ cm^2 c^{-1}, $D_{\mathrm{OH}} = 5.285\times10^{-5}$ cm^2 c^{-1} ([12], 25°C). By assuming that the temperature of the water where the equilibrium concentration of ions is 2×10^{17} cm^{-3} [11] is equal to 200°C, we obtain $N \approx 10^9$, which is almost two orders of magnitude higher than the experimentally observed value of $N = 2\times10^7$. Moreover, if we take this experimental value of N, then in accordance with the calculation the surface temperature of the water should be around 60°C, which certainly does not correspond to the experimental results. This discrepancy indicates that the adopted model does not take into account some important mechanisms, including thermal diffusion. However, there is another important factor that must be taken into account when considering the motion of the charged vapour. It is associated with the fact that an electric field affects the motion of the charge, which was not taken into account in our investigation.

An electric charge, escaping the water surface, is attracted by the charge on the water surface, i.e., it slows down by the electric field. Figure 9 shows the potential difference between the point at which the charge escaping the water surface resides and the water surface, calculated using (7). In the centre of the cylinder, this difference is 12–15 V, i.e., the kinetic energy of charged particles is sufficient to overcome it. If we assume that the velocity of a charged molecule of water moving from the water surface during intense evaporation is equal to the thermal velocity at a temperature equal to the critical value, this energy is ~0.05 eV, which is clearly not enough to overcome the potential difference of 12–15 V.

A possible solution to this contradiction is the assumption that the charge belongs to a particle moving with a thermal velocity, the mass of the particle being much greater than the mass of a single molecule. In other words, the charge moves along with the cluster. The mass of the cluster can be estimated from the known potential difference, which the charged particle overcomes, if we assume the velocity of the particle to be thermal, i.e., this mass should be greater than $300M_{\mathrm{H_2O}}$,

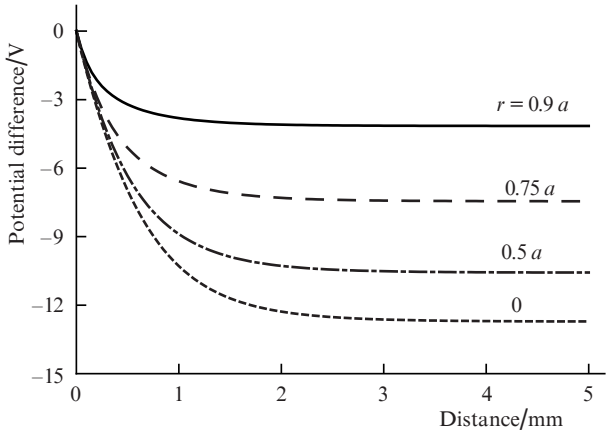

Figure 9. Calculated potential differences between a point above the water surface and the surface on which there is a charge measuring 3.3×10^{-12} C as functions of the distance from the axis of the cylinder of radius 2.5 mm. In the calculation use was made of expression (7).

where $M_{\mathrm{H_2O}}$ is the mass of the water molecule. Under this assumption we can explain the fact that the flying charge is two orders of magnitude smaller than the calculated charge, if use is made of the diffusion mechanism of charge separation, because only clusters can overcome the potential barrier, and all the charges that do not belong to sufficiently massive particles will return to the water surface. This leaves open the question of the place of the formation of clusters: either clusters escape the water surface during evaporation, or vapour condenses in clusters on the charge as in a cloud chamber (see, for example, [15]). This question requires a separate study.

8. Conclusions

The developed method of measuring the electrical signal produced under irradiation of the water surface by high-power IR laser pulses made it possible:

1) to construct a qualitative picture of an electric signal, which is due to the charge motion above the surface of the water;

2) to measure the magnitude of the charge and its sign (the positive charge remains on the water surface and the negative charge flies away);

3) to conclude that the charge separation occurs at the interface between two phases of water (liquid – vapour);

4) to suggest a possible mechanism for the appearance of the first peak of the electrical signal, which leads to the formation of the complex motion of charged vapour near the water surface (of type of 'toroidal vortex') because of the limited size of the laser spot on the water surface; and

5) to conclude that the charges moving in a pair belong to clusters whose mass is more than 300 times greater than the mass of the water molecule.

Acknowledgements. This work was supported by the Russian Foundation for Basic Research (Grant Nos 12-02-00641-a, 12-02-00465-a and 10-02-00770-a), as well as by the President Grant for Government Support of the Leading Scientific Schools of the Russian Federation (Grant No.NSh-368.2012.2).

Appendix

The above expression (3) for the coefficients A_n was obtained for the case of a discontinuous distribution of the charge density. The validity of the expansion of such a charge density into Bessel functions may cause some doubt. To dispel it, we present below a solution for continuous radial distribution of the charge density for which the expansion into Bessel functions is certainly valid. Let the radial distribution of the charge density be given by

$$\sigma(r) = \frac{q(\mu+1)}{S_a}\left[1-\left(\frac{r}{a}\right)^2\right]^{\mu}, \quad \mu > -1, \quad r \leqslant a. \tag{A1}$$

This distribution is continuous, and $\sigma(a) = 0$. If $\mu \to 0$, then it transforms into the above uniform distribution.

In the plane $z = z_1$ there is a free charge with the surface density defined by equation (A1). The jump in the normal component of the induction $D_n(r, z)$ on this surface will have the form:

$$D_n(r, z = z_1 + 0) - D_n(r, z = z_1 - 0) = \sigma(r),$$

where

$$D_n(r, z = z_1 + 0) = -\varepsilon_1\varepsilon_0 \frac{\partial U(r,z)}{\partial z}\bigg|_{z=z_1+0} \quad \text{at } z_1 > z_0.$$

From (2) we obtain

$$-\varepsilon_1\varepsilon_0\left(\frac{\partial U_0(r, z-z_1)}{\partial z}\bigg|_{z=z_1+0} - \frac{\partial U_0(r, z-z_1)}{\partial z}\bigg|_{z=z_1-0}\right) = \sigma(r).$$

By substituting in the above expression the expansion $U_0(r, z - z_1)$ from (2), we obtain

$$2\varepsilon_1\varepsilon_0 \frac{1}{a}\sum_{n=1}^{\infty} A_n\gamma_n J_0\left(\gamma_n \frac{r}{a}\right) = \sigma(r). \tag{A2}$$

Let us multiply the right and left sides of (A2) by $J_0(\gamma_n r/a)$ and integrate them over the radius within [0, a] with weight r. Consider that

$$\int_0^1 x(1-x^2)^{\mu} J_0(bx)\,\mathrm{d}x$$

$$= 2^{\mu}\Gamma(\mu+1)b^{-(\mu+1)}J_{\mu+1}(b), \ b > 0, \ \mu > -1 \ [16, \text{p.}702],$$

and then for the coefficients A_n we obtain

$$A_n = a\frac{q(\mu+1)2^{\mu}\Gamma(\mu+1)\gamma_n^{-(\mu+2)}J_{\mu+1}(\gamma_n)}{S_a\varepsilon_0 J_1^2(\gamma_n)}. \tag{A3}$$

When $\mu \to 0$, (A3) transforms into (3), which was the aim of this proof.

The case when the charge lies on the surface of the interface between two media, i.e., $z_1 = z_2$, should be considered separately. However, if we use (2), the result will be the same.

References

1. Il'ichev N.N., Kulevskii L.A., Pashinin P.P. *Kvantovaya Elektron.*, **35** (10), 959 (2005) [*Quantum Electron.*, **35** (10), 959 (2005)].
2. Andreev S.N., Il'ichev N.N., Kazantsev S.Yu., Kononov I.G., Kulevskii L.A., Pashinin P.P., Firsov K.N. http://zhurnal.ape.relarn.ru/articles/2006/094.pdf.
3. Andreev S.N., Il'ichev N.N., Kazantsev S.Yu., Kononov I.G., Kulevskii L.A., Pashinin P.P., Firsov K.N. *Laser Phys.*, **17** (8), 1041 (2007).
4. Andreev S.N., Kazantsev S.Yu., Kononov I.G., Pashinin P.P., Firsov K.N. *Kvantovaya Elektron.*, **40** (8), 716 (2010) [*Quantum Electron.*, **40** (8), 716 (2010)].
5. Andreev S.N., Kulevskii L.A. *Prikl. Fiz.*, (4), 30 (2008).
6. Samokhin A.A. *Kvantovaya Elektron.*, **1** (9), 2056 (1974) [*Sov. J. Quantum Electron.*, **4** (9), 1144 (1974)]
7. Shamokin A.A., Vovchenko V.I., Il'ichev N.N., Shapkin P.V. *Laser Phys.*, **19** (5), 1187 (2009).
8. Bandura, A.V., Lvov S.N. *J. Phys. Chem. Ref. Data*, **35**, 15 (2006); http://www.iapws.org/relguide/Ionization.pdf
9. Melvin-Hughes E.A. *Ravnovesie i kinetika reaktsii v rastvorakh* (Equilibrium and Kinetics of Reactions in Solutions) (Moscow: Khimiya, 1975).
10. Vodop'yanov K.L., Kulevskii L.A., Mikhalevich V.G., Rodin A.M. *Zh. Eksp. Teor. Fiz.*, **91** (1), 114 (1986).
11. Vodop'yanov K.L. *Zh. Eksp. Teor. Fiz.*, **97** (1), 205 (1990).
12. Vodop'yanov K.L., Kulevskii L.A., Maznev A.A. *Trudy IOFAN*, **28**, 82 (1991).
13. Fernandez D.P., Goodwin A.R.H., Lemmon E.W., Levert Sengers J.M.H., Williams R.C. *J. Phys. Chem. Ref. Data*, **26**, 1125 (2006); http://www.iapws.org/relguide/dielec.pdf
14. Wood R.W. *Nature*, **63**, 418 (1901).
15. Das Gupta N.N., Ghosh S.K. *Usp. Fiz. Nauk*, **31** (4), 491 (1947).
16. Gradshteyn I.S., Ryzhik I.M. *Tablitsy integralov, summ, ryadov i proizvedenii* (Tables of Integrals, Series, and Products) (Moscow: Fizmatgiz, 1962).